Research Square

Preprints are preliminary reports that have not undergone peer review.
They should not be considered conclusive, used to inform clinical practice,
or referenced by the media as validated information.

Impact Hammer Selection for Resonance Testing of Bituminous Mixture Slabs: Experimental and Numerical Investigation

Ana Karoliny Lemos Bezerra

ana.bezerra@det.ufc.br

ENTPE, Ecole Centrale de Lyon, CNRS, LTDS, UMR5513

Jean-Claude Carret

École de Technologie Supérieure (ÉTS)

Salvatore Mangiafico

ENTPE, Ecole Centrale de Lyon, CNRS, LTDS, UMR5513

Cédric Sauzéat

ENTPE, Ecole Centrale de Lyon, CNRS, LTDS, UMR5513

Research Article

Keywords: Frequency Response Function, Flexural vibration modes, Instrumented hammer, Viscoelastic characterization, Asphalt materials

Posted Date: November 25th, 2026

DOI: https://doi.org/10.21203/rs.3.rs-11394150/v1

License: This work is licensed under a Creative Commons Attribution 4.0 International License.
Read Full License

Additional Declarations: No competing interests reported.

Impact Hammer Selection for Resonance Testing of Bituminous Mixture Slabs: Experimental and Numerical Investigation

Ana Karoliny LEMOS BEZERRA[1] [0000-0002-9540-0837] · Jean-Claude CARRET[2] [0000-0002-2081-5165] · Salvatore MANGIAFICO[1] [0000-0003-0548-6989] · Cédric SAUZÉAT[1] [0000-0001-5055-8887]

[1] ENTPE, Ecole Centrale de Lyon, CNRS, LTDS, UMR5513, 69518 Vaulx-en-Velin, France
[2] École de Technologie Supérieure (ÉTS), Montréal, QC, Canada

Corresponding author: Ana Karoliny LEMOS BEZERRA, ana.bezerra@det.ufc.br

Abstract

Purpose: This experimental and numerical study investigates how hammer characteristics influence the vibration modes and frequency response of bituminous mixture slabs during Impact Resonance Test (IRT) measurements. **Methods:** IRT measurements were performed on two rectangular slabs with different thicknesses using a miniature steel hammer and a regular impact hammer equipped with interchangeable steel, plastic, soft plastic, and super-soft plastic tips. Force and acceleration signals were analysed in the time and frequency domains to obtain Frequency Response Functions (FRFs). Three-dimensional numerical simulations based on a linear viscoelastic model was used to identify vibration modes and validate the experimental responses. **Results:** Hammer mass and tip stiffness influenced the excitation bandwidth and the identification of slab vibration modes. The regular hammer with plastic and steel tips provided suitable frequency content within 0–3000 Hz, allowing identification of the first two flexural modes. The miniature steel hammer provided limited excitation at low frequencies, whereas the super-soft tip concentrated energy at very low frequencies. Experimental and numerical results showed good agreement, confirming the identified vibration modes. The regular hammer with the plastic tip was the most suitable configuration for the investigated this type of material and geometry. **Conclusion:** Hammer selection is important in IRT measurements on rectangular bituminous mixture slabs because it determines the excitation of vibration modes and the quality of the measured frequency response. The combined experimental and numerical approach supports the interpretation of the responses and the selection of suitable excitation systems for the dynamic viscoelastic characterization of bituminous mixtures.

Keywords: Frequency Response Function · Flexural vibration modes · Instrumented hammer · Viscoelastic characterization · Asphalt materials

Acknowledgments

The authors acknowledge funding from the European Union's Horizon Europe programme under the Marie Skłodowska-Curie Grant Agreement No. 101072820 (CIRCOPAV project) and from Bauval for providing the bituminous materials.

1 Introduction

Non-destructive testing (NDT) techniques have become increasingly important for the mechanical characterization of bituminous mixtures, particularly for evaluating their linear viscoelastic behavior without damaging the specimen [1-6]. Among these techniques, the Impact Resonance Test (IRT) has emerged as a reliable NDT alternative. In IRT, an external mechanical impact generates elastic waves within the specimen, and the resulting dynamic response is governed by the propagation of elastic waves within the specimen, which depends on the material properties, specimen geometry, density and boundary conditions. Consequently, the measured resonance frequencies and vibration modes are directly related to parameters such as the complex modulus, Poisson's ratio and material damping. With the introduction of instrumented impact hammers equipped with load cells, it became possible to simultaneously acquire the excitation force and the vibrational response, allowing the determination of

Frequency Response Functions (FRFs), which constitute the basis for recently advanced modal identification and inverse analysis techniques developed for bituminous mixtures [4-5, 7-9].

The experimental configuration adopted in IRT has evolved considerably over the last decades. Early studies generally employed simple manual excitation systems, such as metallic sphere balls or impact devices adapted from procedures originally developed for elastic materials [10-11]. Although these approaches remain in use [3, 12], several efforts have been made to improve excitation repeatability and measurement quality. Ryden (2009) [13] proposed a miniature impact hammer consisting of a steel bar attached to a plastic strip, while [14] introduced a guided steel sphere system to improve impact consistency. The subsequent development of instrumented hammers represented a major advance, enabling the direct measurement of both input and output signals and, consequently, the calculation of FRFs with greater reliability. This evolution considerably expanded the possibilities of modal characterization and inverse numerical analysis of bituminous materials.

Since the FRF represents the relationship between the input excitation and the structural response over the frequency domain, its quality strongly depends on the characteristics of the impact excitation. The force spectrum generated during impact is influenced by the hammer mass, the stiffness of the tip material, and the contact duration between the hammer and the specimen. Because the stiffness of the tested material cannot be modified during the experiment, the excitation frequency range can be controlled primarily through the selection of the hammer configuration, which determines the amount of energy transmitted at different frequencies. Consequently, the hammer tip plays a decisive role in defining which resonant modes are effectively excited and identified in the measured FRF, directly affecting the interpretation of the dynamic behavior of the material.

Several studies have demonstrated that the characteristics of the impact hammer significantly influence the quality of dynamic measurements. Zahari et al. (2011) [15], although investigating thin aluminum plates, showed that the stiffness of the hammer tip directly controls the excited frequency bandwidth and, consequently, the vibration modes identified during modal analysis. By comparing hard, medium, soft and super-soft hammer tips, the authors concluded that selecting an appropriate tip is essential for obtaining reliable modal parameters. Similar conclusions were reported by [16], who evaluated metal, plastic and rubber hammer tips on solid rectangular plates using experimental modal analysis based on impact excitation, accelerometers, Fast Fourier Transform (FFT) processing and FRF calculation. Among the tested configurations, the plastic tip provided the most suitable excitation bandwidth, covering frequencies up to approximately 3 kHz. Their study also showed that, although the excitation location affects the response amplitude, it does not modify the natural frequencies of the structure.

More recently, [17] investigated different excitation configurations in impact-echo testing, a technique based on physical principles similar to those of IRT. The study compared blunt and sharp hammer tips, with and without hammer handles, on concrete and reinforced concrete elements. Rather than recommending a single optimal configuration, the authors proposed a signal quality evaluation methodology supported by machine learning techniques, highlighting that the choice of excitation system substantially affects the quality and interpretation of the measured response.

Although these investigations have demonstrated the importance of hammer characteristics for modal testing, they were mainly conducted on metallic or concrete structures, whose mechanical behavior differs substantially from that of bituminous mixtures. Asphalt mixtures exhibit viscoelasticity behavior, heterogeneous and high material damping, all of which influence wave propagation and energy dissipation during impact loading [18-19]. Moreover, the dynamic response of slab specimens represents a more complex problem than that of homogeneous media, since it depends simultaneously on the mechanical properties of the material, specimen geometry, boundary conditions, excitation frequency

and the interaction between different wave propagation modes. Consequently, conclusions obtained for metallic or concrete structures cannot be directly extended to asphalt mixture slabs.

Despite the growing application of IRT for the characterization of bituminous materials, the influence of hammer configuration on the measured frequency response remains insufficiently understood. Previous investigations have demonstrated that hammer mass and tip stiffness affect the excited frequency bandwidth and the quality of modal identification, but these studies were primarily conducted on metallic or concrete structures. Consequently, the extent to which these findings can be transferred to highly viscoelastic bituminous mixture slabs remains unclear. Furthermore, although finite element modelling has become an important tool for supporting experimental analyses, relatively few studies have combined experimental IRT measurements with numerical simulations to explain how different hammer configurations influence the excitation of resonant modes and the resulting FRFs. Such an integrated approach is particularly relevant for bituminous mixtures, where the interaction between wave propagation, material damping and geometry produces a more complex dynamic response than that observed in conventional elastic materials.

In this context, this study investigates the influence of different impact hammer configurations on the frequency response of rectangular bituminous mixture slabs during IRT measurements. Experimental tests were performed using instrumented hammers equipped with different tip materials in order to evaluate how hammer characteristics determine which resonant modes are effectively excited and observable in the FRF, and how this influences the interpretation of the material's viscoelastic behavior. The experimental investigation was complemented by numerical simulations study based an linear viscoelastic model to support the interpretation of the measured responses and to validate the vibration modes excited under different impact conditions. Two bituminous mixture slabs with different thicknesses were investigated to assess the repeatability and to verify the results obtained from the experimental and numerical analyses.

2 Experimental campaigns

This section presents the materials and methods adopted for the investigation of rectangular bituminous mixture slabs. It first describes the materials used and the experimental IRT setup, including the slab geometry, testing procedure, measurement positions, and the different impact hammer configurations investigated. It then presents the numerical methodology, describing the finite element model developed to simulate the slab dynamic response.

2.1 Materials

Two rectangular slabs of the bituminous mixture, 60 x 40 x 15 cm (compaction mold), were compacted using a French wheel compactor, in a single layer. Each slab was compacted to a different height, as can be seen in Fig. 1, and are designated in this work as SL-7 and SL-11, where SL=Single layer. One hot-mix bituminous mixture, very common in Quebec for pavement structures, were used for the two slabs: an ESG-10 ("*Enrobé Superficiel Granulaire*", in French) which is a dense-graded surface mixture with a nominal maximum aggregate size of 10 mm (gradation 0/10). The PG 64H-28 binder used in the mixtures followed the PG (Performance Grade) classification system. In this nomenclature, the number 64 represents the high-temperature grade (in °C) at which the binder maintains adequate rutting resistance, and –28 indicates the low-temperature grade associated with its ability to resist thermal cracking. The letters H and E denote the expected traffic loading level on the pavement, with H (Heavy) corresponding to high traffic and E (Extreme) to very heavy traffic conditions.

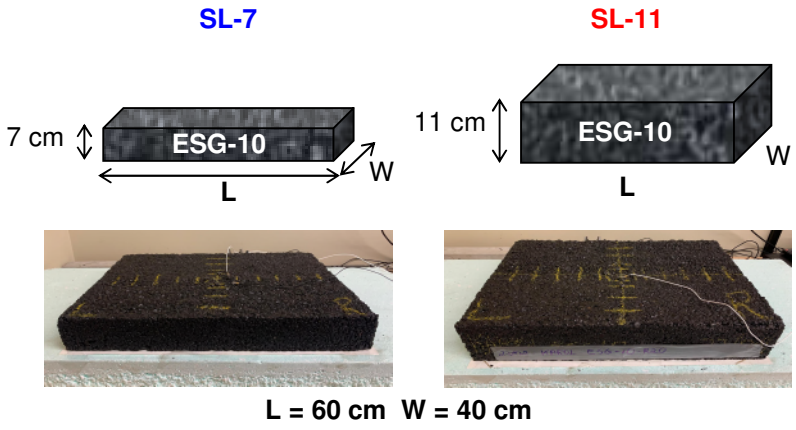

Fig. 1 Representation of the compacted and tested slabs

The bituminous mixture was provided by the Bauval company, where the aggregates and bitumen were already mixed. At the ETS laboratory they were only heated to 160°C and compacted, in accordance with the recommendation of the Quebec standard LC 26-400 [20] for each bitumen type. After compaction and curing, after two days, the air void was calculated geometrically (see Eq. 2) with the Maximum Specific Gravity (Gmm) provided by the mixture company used together with the Apparent Specific Gravity (Gmb) (Eq. 1) and with the average height from twenty-four measurements of the slab.

$$\boldsymbol{Gmb\ (kg/m^3) = \frac{m}{\pi H D^3/4}} \quad (1)$$

$$Void\ content\ (\%) = 1 - \frac{Gmb}{Gmm} * 100 \quad (2)$$

Measurements were taken uniformly across the entire surface, as shown in Fig. 2. An aluminum bar was positioned transversely across the compaction mold, serving as a stable reference plane. The digital caliper was then placed vertically on this bar, allowing its depth rod to reach the surface of the compacted mixture. For each measurement point, the Hx reading (distance between the reference bar and the surface of the mixture) was recorded, while the total reference height HT was measured separately. The actual slab thickness at each point (Hp) was obtained as Hp = HT – Hx. This procedure ensured a reliable assessment of thickness variability across the slab. Table 1 shows the main characteristics of the slabs used in this study in terms of geometric dimensions, mass, real density (Gmm) and void content.

Table 1 Concise table title explaining the table contents

Slab	Mass (kg)	Length (mm)	Width (mm)	Height (mm)	Gmm (kg/m3)	Void content (%)
SL-7	39.96	600	400	74.29	2.503	10.47
SL-11	62.43			114.05		8.88

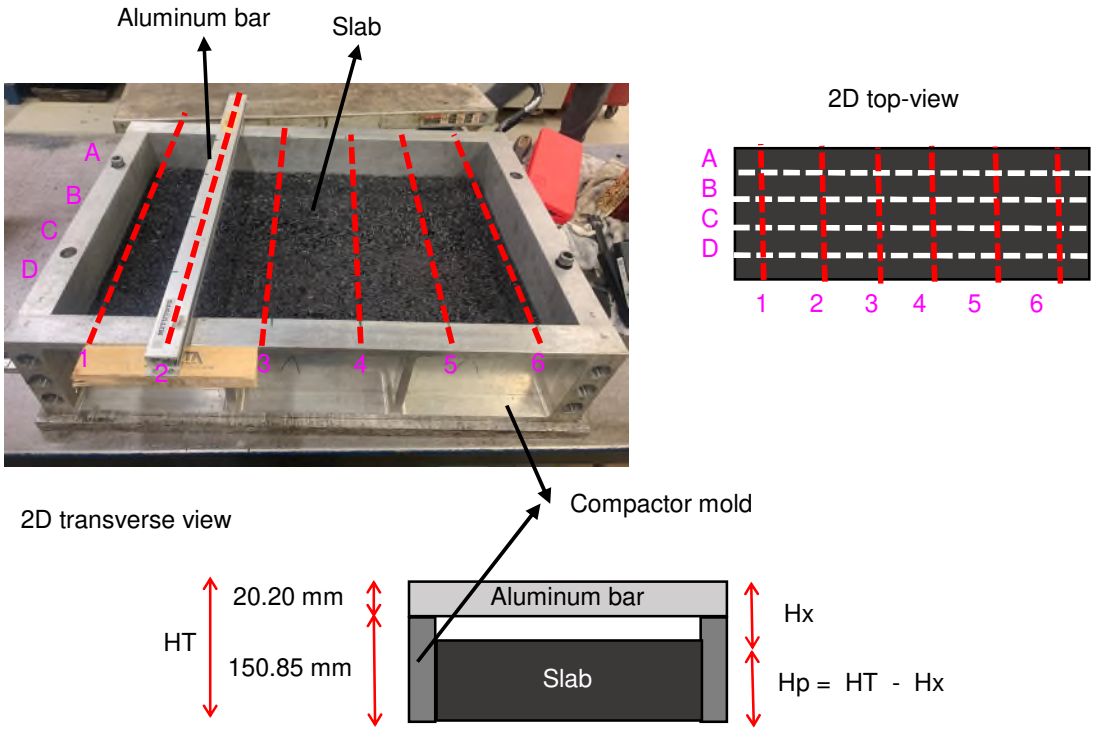

Fig. 2 Schematic representation for measuring the height of the slabs

2.2 Impact Resonance Test

The IRT test set-up and impact hammers used in this study are shown in Fig. 3 and Fig. 4, respectively. The IRT was performed considering the flexural vibration mode with both the impact hammer and the accelerometer were placed at the top surface of the slab. Five manual impacts were performed in the middle of the surface slab, and a uniaxial accelerometer (PCB model 353B15) was used to measure the excitation caused by the impacts at different positions, as can be seen in Fig. 3b, totaling twenty measurements. Measurements were taken at 3, 5, 10, 15, 20, and 25 cm at the up (U), down (D), to the left (L), and to the right (R) of the center of the slab (where the impact was made). For each test position, the accelerometer was fixed to its mounting base, which was glued to the surface of the slab. Only after the electronic system had completely stabilized, which can take around 5-8 min, the impacts were initiated. As you can see in Fig. 3a, the slab was placed on 10 cm thickness polystyrene foam in order to minimize boundary effects and allow vibration modes closer to free boundary conditions. The foam with the slab was placed on a stable wooden table with no risk of vibration of the system during the test.

Regarding the hardware, the data acquisition system was NI model USB-634. This device offers a maximum sampling rate of 500 kHz for all channels, corresponding to one data point every 2×10^{-6} second, but also sufficient for good measurement accuracy. The test was performed using Python software developed specifically for this application test.

In order to investigate which, type of hammer is most suitable for this type of test configuration proposed in this second experimental campaign, two hammers were used: a miniature hammer (SH), model PCB 086E80, and a regular hammer (RH), model PCB 086C02. Both integrate a quartz force sensor in the hammer head, which converts the impact force into a proportional electrical signal. The sensor operates with constant current excitation (2–20 mA). Fig. 4 show the impacts hammer and their tips and their main differences. The SH is a lightweight mini hammer (mass of 4.8 g and length of 107 mm) equipped with a hard-stainless steel tip. The RH is a regular hammer (mass of 0.16 kg and length of 234 mm) supplied with interchangeable tips of different stiffness, allowing adjustment of the impact bandwidth. The main distinction between the hammers is the difference in resonant frequency sensitivity. According

to the PCB specification, the SH can work with high frequencies up to 100 kHz and the RH up to 22 kHz, depending on the material of the hammer's tip.

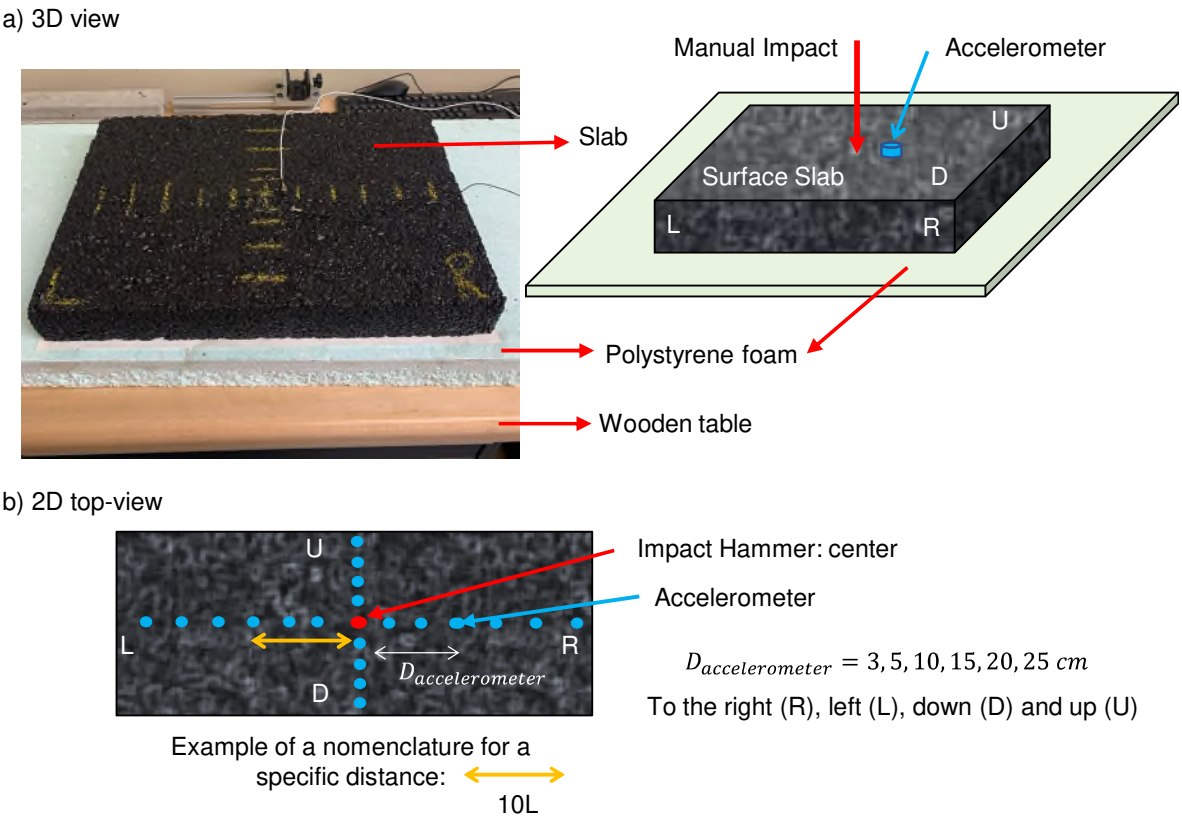

Fig. 3 Set-up of the IRT in flexural vibration mode on a rectangular slab: a) 3D view set-up; b) 2D top-view of the locations of impact and accelerometer on the surface of the slab

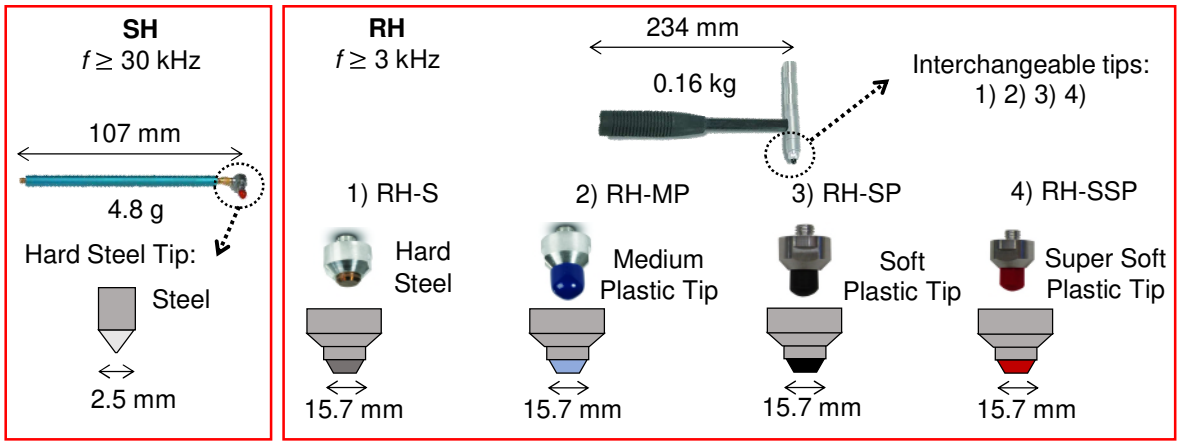

Fig. 4 Two types of hammers used (SH miniature hammer and RH regular hammer) and the different tips used in the IRT on a rectangular slab

For the RH, four tips were used, identified as: (i) the hard stainless steel (RH-S), model 084B03, which provides the highest contact stiffness, generating short-duration impacts with a broad frequency content and higher force amplitudes; (ii) the medium plastic tip (RH-MP), model 084B04, which provides a moderate level of stiffness, balancing the force amplitude and frequency range; (iii) the soft in black (RH-SP), model 084C05, which produces lower contact stiffness, leading to longer impact durations and concentrating the excitation toward mid- to low-frequency ranges; (iv) the super soft in red (RH-

SSP), model 084C11, which offers the lowest stiffness among the tested configurations, resulting in the longest contact time and predominantly exciting the lower frequencies of the specimen. The test temperature was around 23°C, which is the constant ambient temperature of the room where the test was performed.

To investigate the influence of the impact hammer on the dynamic response of rectangular bituminous mixture slabs, a series of IRT tests was carried out using two slabs (SL-7 and SL-11) at 23 °C and the hammers showed in Fig. 4. An initial and more comprehensive investigation was performed on slab SL-7, where the SH and RH-MP hammers were tested at all measurement positions, while the RH-S, RH-SP and RH-SSP hammers were evaluated at selected positions (3U,3D,3L,3D 5U,5D,5L,5D) representative of the central and peripheral regions of the slab. Based on these results obtained with the first slab tested (SL-7), three hammers (SH, RH-MP and RH-S) and specified positions (3L,3D,5L,5D) were chose to test on slab SL-11 for verify the repeatability of the observed previous trends. The RH-S and SH hammers were tested only in positions 3L, 3D, 5L, 5D on slab SL-11 and the RH-MP in all positions (3U,3D,3L,3D,5U,5D,5L,5D,10U,10D,10L,10D,15U,15D,15L,15D, 20R, 20L, 25R and 25L) for slab SL-7 and SL-11. This experimental strategy reduced the total number of tests while allowing the main conclusions regarding hammer performance to be verified on a second slab with a different thickness.

About data processing, in summary, after the IRT tests, data are obtained in the time domain: acceleration for the output signal measured by the accelerometer and force signal for the input signal obtained by the load cell attached to the tip of each hammer. With the Fast Fourier Transform (FFT), the signals in the time domain are converted into signals in the frequency domain. With this, the Frequency Response Function (FRF) is calculated as the ratio between the FFT of the force and the FFT of the acceleration, according to Eq. 3.

$$\boldsymbol{FRF(f)} = \frac{\overline{\boldsymbol{X^*(f).Y(f)}}}{\overline{\boldsymbol{X^*(f).\ X(f)}}} \tag{3}$$

where X and Y are the FFT of the applied force and acceleration, X* is the complex conjugate of the force, and the bars denote the average of the five impacts.

Also, as in [5, 7], the Coherence Function (CF) is used as quality indicator of the FRFs measurements. This function evaluates the correlation between the input and output signals at each frequency. The coherence is a real function that ranges between zero and one. A value of one indicates that the output is fully explained by the input, while decreasing values mean there is noise in the system that has disrupted the test. Values between 0.7 to 1 in the frequency range that contains the resonance frequency peaks can be used, but tests presenting CF values below 0.7 should be excluded. The coherence function is calculated with Eq. 4.

$$\boldsymbol{CF\ (f)} = \frac{|\overline{\boldsymbol{X^*(f)\ .\ Y(f)}}|^{\boldsymbol{2}}}{\overline{\boldsymbol{X^*(f)\ .X(f)}}\ .\ \overline{\boldsymbol{Y^*(f)\ .Y(f)}}} \tag{4}$$

3 Numerical study

The numerical model was implemented using the commercial FEM software COMSOL. The main response obtained from the numerical simulations is the numerical FRF. Fig. 5 illustrates the conditions used for calculating the numerical FRF with FEM for the defined three-dimensional geometry (3D), as

well as the impact point location, and the different accelerometer locations considered. Rectangular slabs with 40 cm width, 60 cm length and 7.4 and 11.4 thickness were modeled.

For the mesh definition, a mesh study was conducted to define the mesh with the best cost-benefit ratio in terms of computational time and response consistency with the experimental results. For this purpose, two types of elements (tetrahedral and quadrangular) and different maximum element sizes were tested. The converged mesh was the tetrahedral element mesh with a maximum element size of 0.022 m.

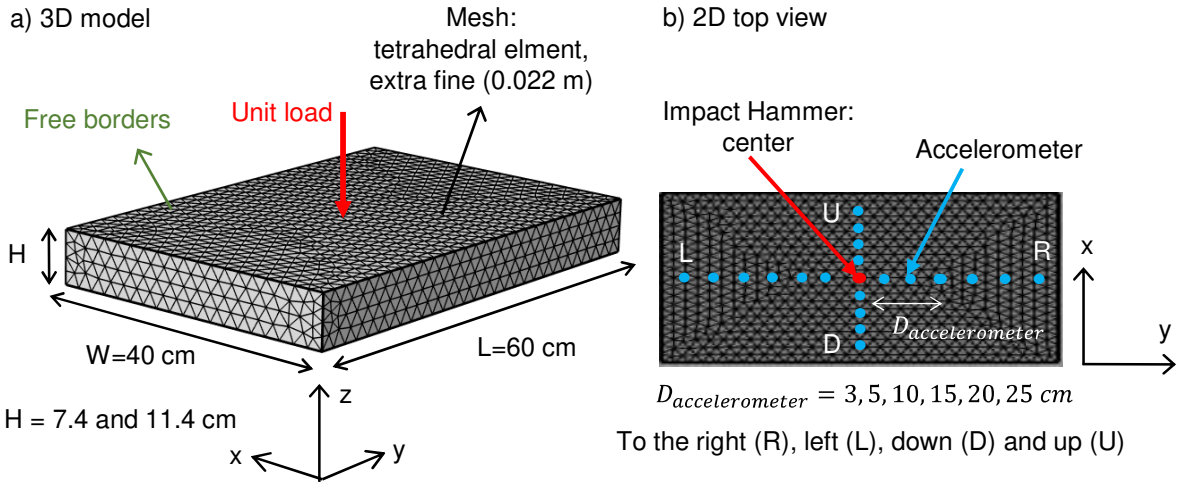

Fig. 5 Numerical model on rectangular slab: a) 3D geometry; b) top-view with positions measurements

Since experimentally the slab is placed on top of a foam (See Fig. 3), free boundary conditions were considered, except at the impact location, where a unit cyclic load is applied in the direction of the impact, following Eq. 5.

$$\boldsymbol{F = e^{i\omega t}} \tag{5}$$

An isotropic linear viscoelastic (LVE) behavior is considered for the bituminous mixture with a complex modulus and a complex Poisson's ratio dependent on frequency and temperature. It is modeled with the 3-dim version of the 2S2P1D model [21-22], as Eq. 6 and Eq. 7. Table 2 presents the values of the 2S2P1D parameters used, derived from [5, 8] reference material and IRT tests for the ESG-10 material. The Apparent Specific Gravity (Gmb) was equal to 2241.04 kg/m³. The simulations were performed at a temperature of 23°C, which is close to the ambient temperature of the laboratory room where the experimental IRT tests were conducted on rectangular slabs, through the insertion of the William Landy-Ferry (WLF) [23] equation (Eq. 8) into the model.

$$\boldsymbol{E^*(\omega) = E_{00} + \frac{E_0 - E_{00}}{1 + \delta(i\omega\tau)^{-k} + (i\omega\tau)^{-h} + (i\omega\beta\tau)^{-1}}} \tag{6}$$

$$\nu^*(\omega) = \nu_{00} + \frac{\nu_0 - \nu_{00}}{1 + \delta(i\omega\tau_\nu)^{-k} + (i\omega\tau_\nu)^{-h} + (i\omega\beta\tau_\nu)^{-1}} \tag{7}$$

$$log\ (a_T) = -\frac{C_1(T - T_{REF})}{C_2 + (T - T_{REF})} \tag{8}$$

where E_{00} represents the static modulus when the frequency approaches 0 ($\omega \to 0$), while E_0 corresponds to the glassy modulus when the frequency approaches infinity ($\omega \to \infty$). The parameters k and h are dimensionless constants associated with the two parabolic elements, typically satisfying $0<k<h<1$. The parameter δ is a dimensionless shape parameter, and β is a dimensionless parameter related to the

Newtonian viscosity η of the dashpot, defined as ($\eta=(E_0-E_{00})\beta\tau$). The angular frequency is denoted by $\omega=2\pi f$ (where f is the loading frequency) and τ dependent on temperature, T is the test temperature, T_{REF} is the reference temperature, and C_1 and C_1 are experimentally determined constants.

Table 2 Concise table title explaining the table contents

Slab	E_{00} (MPa)	E_0 (MPa)	δ	k	h	β	$\tau_{E15°C}$ (s)	ν_{00}	ν_{00}	$\tau_{\nu 15°C}$ (s)	C_1	C_2 (°C)
SL-7	100	29000	1.8	0.15	0.53	250	0.0006	0.19	0.43	3.165	21.2	200.4
SL-11	100	33000	1.8	0.15	0.53	250	0.0006	0.19	0.43	3.165	21.2	200.4

As the applied cyclic load is unitary, the obtained acceleration amplitude corresponds directly to the FRF value. The study parameters in the frequency domain (previously selected in the COMSOL software at the beginning of the model creation) are defined. The frequencies for which the calculations were performed were chosen to match the frequency range accessible with the experimental tests, between 2 Hz and 3 kHz, with a frequency resolution of 1 Hz. However, for the mesh study, a lower frequency resolution was adopted to reduce the computational time. Finally, the model is run and the numerical FRF is calculated by numerically solving the three-dimensional wave motion equation (Eq. 9) in the frequency domain for each specified frequency.

$$-\rho\omega^2\vec{u} - \nabla.\underline{\underline{\sigma}} = 0 \qquad (9)$$

where ρ is the bulk density of the material, ω is the pulsation (equal to 2πf), $\vec{u}$ is the displacement vector, ∇ is the gradient tensor operator and $\underline{\underline{\sigma}}$ is the Cauchy stress tensor.

4 Experimental Results and Discursions

Fig. 6 and Fig. 7 show examples of the time-domain signals results of force and acceleration, respectively, for one position, 5 cm to the left of the impact (5L), for all tested hammers (RH-MP, RH-S, SH, RH-SP and RH-SSP) for slab SL-7. The FFT signals of force and acceleration are plotted in Fig. 8 and Fig. 9, respectively. The results for slab SL-11 of the time and frequency domain presented the same trend.

For the SH hammer, the force pulse presents a short duration ($\Delta t \approx 0.12$ ms), and the corresponding acceleration response exhibits multiple high-frequency components, indicating a wider excitation bandwidth, typical of hard metallic tips. On the other hand, the RH-MP hammer generates significantly higher impact amplitudes (up to ≈ 1000 N) and a longer contact time ($\Delta t \approx 0.67$ ms) compared to the SH, due to its higher mass and the use of a medium-stiffness plastic tip. This longer contact time produces a force signal with lower high-frequency content in the response. The RH-S hammer, which combines the mass of the regular hammer (RH) with a hard-stainless-steel tip, produces impacts with high force amplitudes and relatively short contact duration ($\Delta t \approx 0.32$ ms) when compared to the other RH hammers. As a consequence, its acceleration response presents higher-frequency oscillations than those observed for the RH-MP, although still lower than those of the SH due to the larger hammer mass.

For the hammers with softer tips, RH-SP and RH-SSP, the force pulses become progressively longer and smoother, with lower amplitudes and larger contact times ($\Delta t \approx 3$ ms and $\Delta t \approx 6$ ms, respectively). The acceleration responses present oscillations predominantly at low frequencies and strong attenuation of the high-frequency components, especially for the RH-SSP.

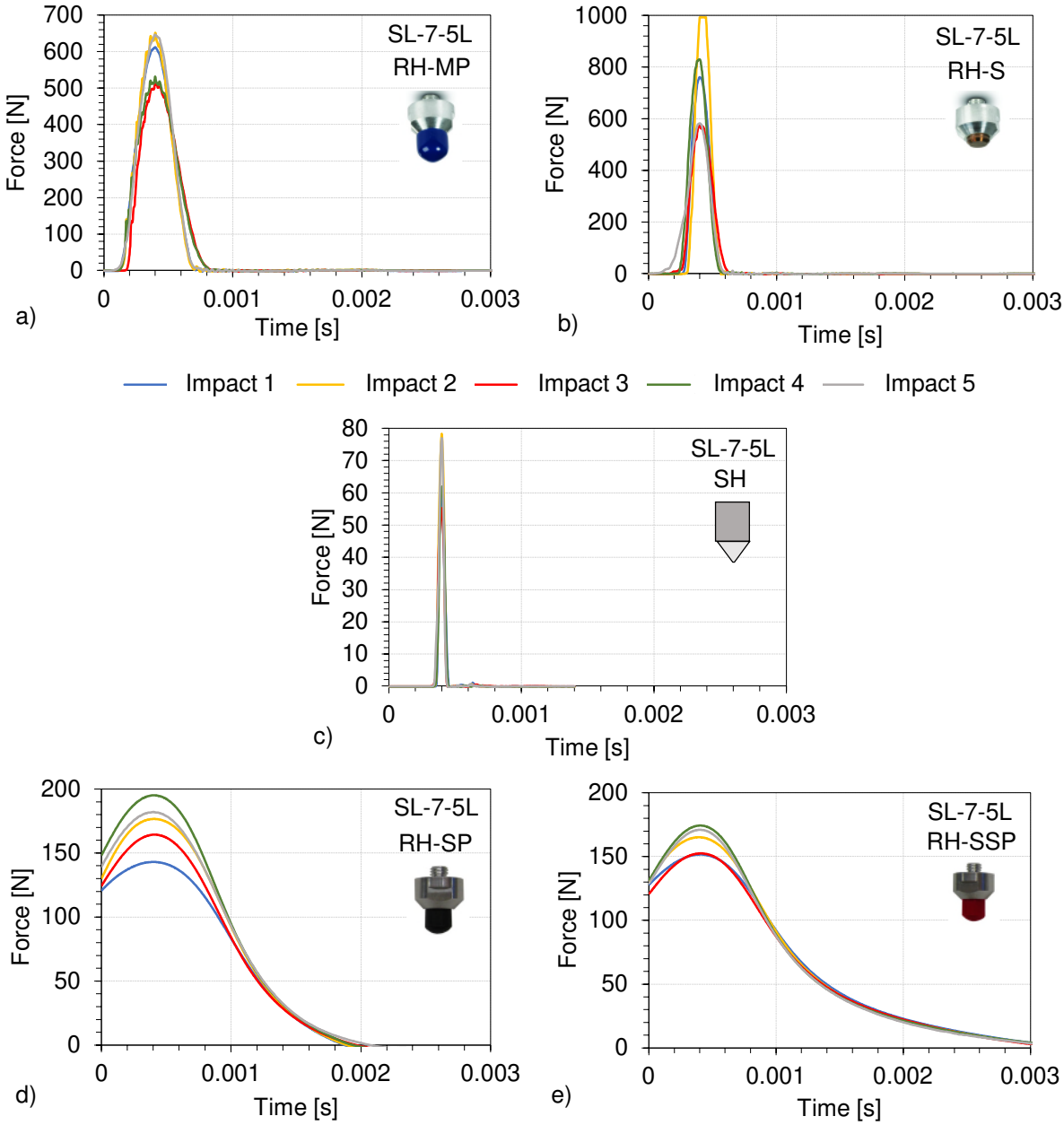

Fig. 6 Five time-domain signals of hammer force for SL-7-5L test with regular hammer (RH) with four impacting tips and small hammer (SH): a) RH-MP; b) RH-s; c) SH; d) RH-SP; e) RH-SSP

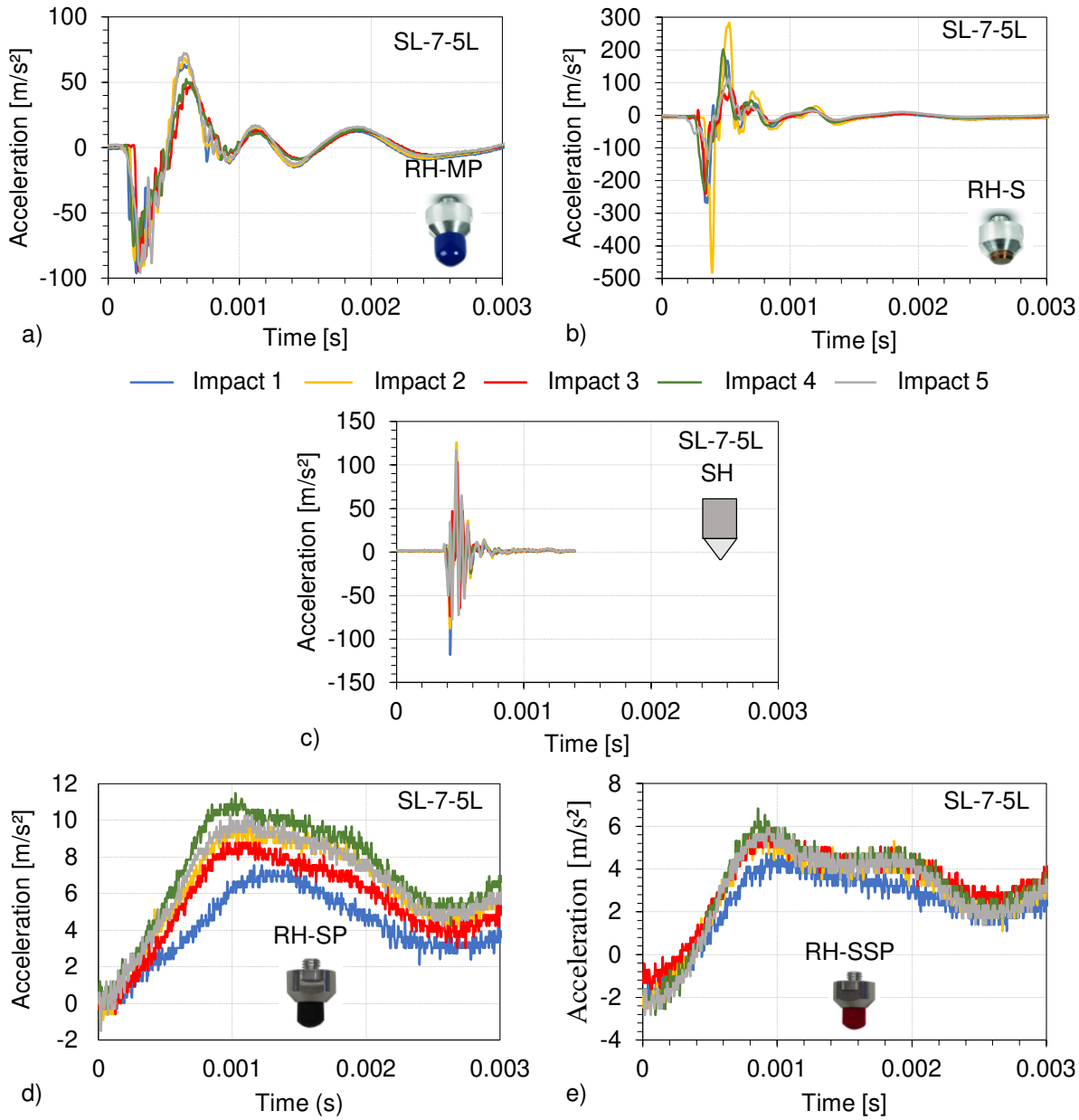

Fig. 7 Five time-domain signals of acceleration for SL-7-5L test with regular hammer (RH) with four impacting tips and small hammer (SH): a) RH-MP; b) RH-s; c) SH; d) RH-SP; e) RH-SSP

The FFT force and acceleration signals (Fig. 8 and Fig. 9) clearly show the differences in excitation bandwidth between the hammers. Based on the force FFT results, it is possible to conclude that the effective excited frequency ranges were approximately: SH (0–20000 Hz), RH-S (0–6000 Hz), RH-MP (0–3000 Hz) and RH-SP/RH-SSP (0–1000 Hz).

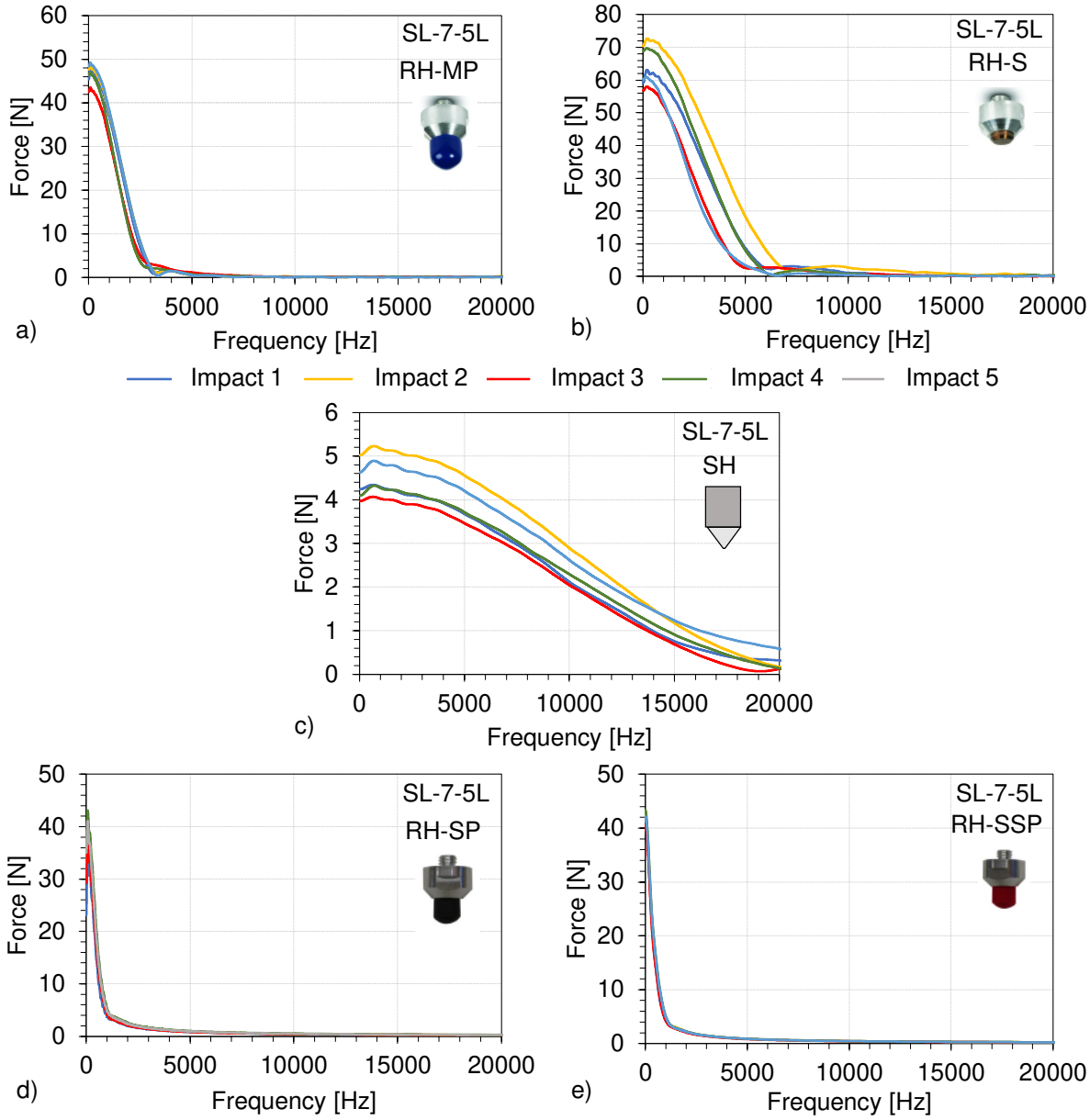

Fig. 8 Five frequency-domain signals of hammer force for SL-7-5L test with regular hammer (RH) with four impacting tips and small hammer (SH): a) RH-MP; b) RH-s; c) SH; d) RH-SP; e) RH-SSP

For the SH, the energy extends up to approximately 30 kHz, reflecting the short contact time and the high stiffness of the metallic tip. In contrast, the RH-MP concentrates most of its energy below approximately 3000 Hz and the RH-S up to 6000 Hz. For the RH-SP and RH-SSP hammers, the frequency content becomes even more concentrated in the low-frequency range. Although the hammer specifications indicate sensitivities up to 100 kHz for SH and 22 kHz for RH, for example, the damping caused by the viscoelastic behavior of the asphalt mixture considerably reduces the effective excitation bandwidth experimentally observed. In addition to the viscoelastic damping of the material, the contact time during the impact and the slab geometry itself also influence this limitation of the effective frequency range. Therefore, despite the nominal capability of the hammers to excite high frequencies, the energy effectively transmitted to the specimen and experimentally observed is concentrated within a lower frequency range.

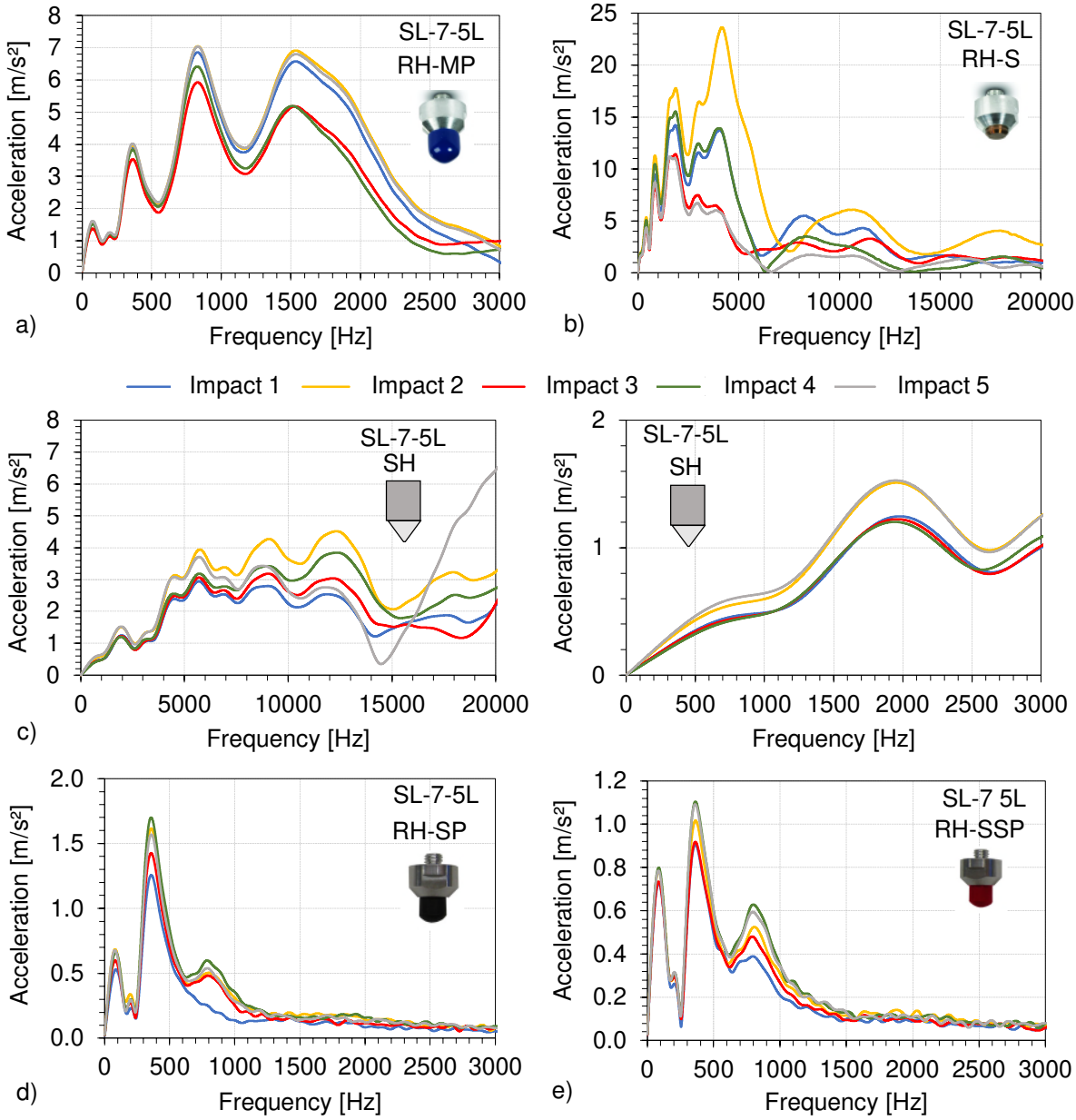

Fig. 9 Five frequency-domain signals of acceleration for SL-7-5L test with regular hammer (RH) with four impacting tips and small hammer (SH): a) RH-MP; b) RH-s; c) SH; d) RH-SP; e) RH-SSP

The results also allow observing the direct influence of the hammer contact time in relation to the acquisition window length and the trigger system used during the tests. The trigger corresponds to the criterion used by the acquisition system to detect the impact signal, normally based on the hammer force signal. When the force exceeds a predefined value (trigger level), the trigger instant is identified. To avoid losing the initial part of the impact, a pre-trigger buffer was used, allowing a small portion of the signal before the trigger instant to be stored.

The record length defines the total duration of the acquisition time window. In this study, a total acquisition time of 3 ms was used, including both the pre-trigger interval and the period after the impact. Thus, the observed signal behavior depends directly on the relationship between the hammer contact time and the available temporal acquisition window.

Hammers with hard tips, such as the SH, produce short-duration pulses, causing the force signal to rapidly return to zero and to be completely captured within the acquisition window. For this reason, the accelerometer response also presents a shorter duration in the time domain. In contrast, the RH-SP and

RH-SSP hammers present significantly longer contact times due to the low stiffness of their tips. In these cases, part of the force signal exceeds the 3 ms temporal window, resulting in the apparent truncation observed in the time-domain signals. However, this truncation does not compromise the FRF determination. Most of the impact energy is concentrated in the initial peak of the force pulse, which is completely recorded within the acquisition window. Since the FRF is calculated from the ratio between the response and excitation spectra, small losses in the final portion of the signal, where the amplitudes are already reduced, have limited influence on the relevant spectral content. Therefore, the observed behavior does not represent an acquisition error, but rather a direct consequence of the interaction between the hammer contact time and the temporal window length adopted in the test execution software.

For a better visualization of the differences between the time-domain responses of the investigated hammers, the graph shown in Fig. 10 was plotted. The data from Fig. 6 presented above for the 5L distance were used, excluding the data corresponding to the pre-trigger. The results correspond to the average of the five impacts. Fig. 10a presents the results for the remaining time of the record length. In Fig. 10b and Fig. 10c, the force was normalized with respect to the maximum peak force of the average of the five impacts for each hammer, in order to better visualize the difference along the x-axis regarding the contact time of each hammer, since the force magnitude differs significantly between the hammers.

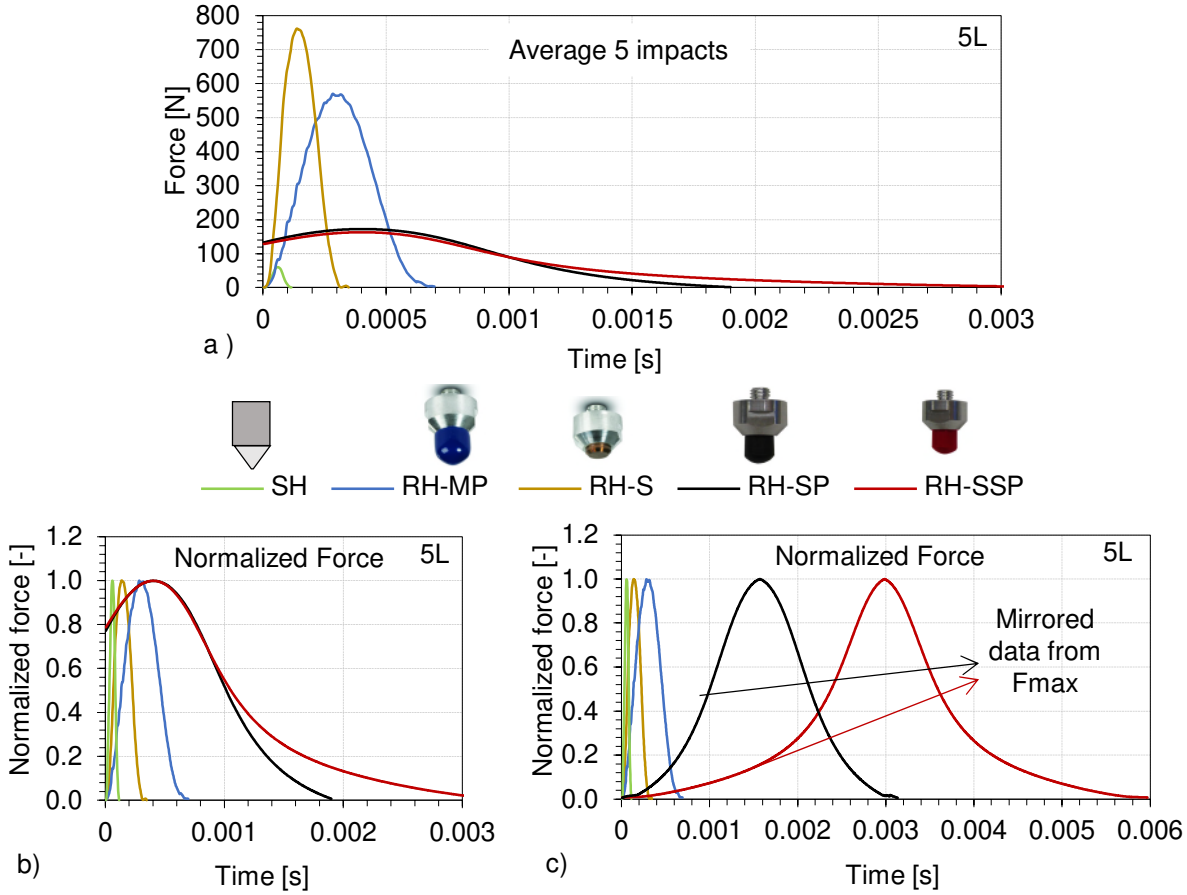

Fig. 10 Comparison of impact force signals in the time domain for all hammers tested, average of five impacts presented in Fig. 6 for SL-7-5L test using regular hammer (RH) with four impacting tips and small hammer (SH): a) total duration of the record length; b) signals normalized relative to the maximum force; c) signals normalized with a mirrored representation of the force pulses from the RH-SP and RH-SSP

The results in Fig. 10c for the RH-SP and RH-SSP hammers were truncated after the maximum peak and mirrored in order to show the complete force pulse and thus allow direct visualization and comparison of the contact time relative to the other hammers. Fig. 10 confirms the results previously discussed, where the hammers can be classified in increasing order of contact time according to the following scale: SH (~ 0.12 ms) < RH-S (~ 0.32 ms) < RH-MP (~ 0.67 ms) < RH-SP (~ 3 ms) < RH-SSP (~ 6 ms).

The Fig. 11 show the FRFs results for all tested hammers for positions 3U and 5L for slab SL-7 and Fig. 12 the FRFs results for SH and RH-MP hammers for positions 3U and 5L for slab SL-11. The FRFs obtained with the SH, RH-MP and RH-S hammers are similar for frequencies higher than 1000 Hz, but they differ for lower frequencies. Indeed, FRFs obtained with the RH-MP and RH-S exhibit two well-defined peaks below 1000 Hz that are not visible on the FRFs obtained with the SH hammer. It indicates that only the RH-MP and RH-S can be used to efficiently excite the natural flexural modes of the bituminous mixture slabs for this frequency range study (0–3000 Hz). Using the SH hammer can lead to a misinterpretation of the results, as the first visible peak does not correspond to the fundamental flexural frequency. These findings are consistent with [16-17, 24], who demonstrated that both tip stiffness and hammer mass determine the effective excitation bandwidth and the vibration mode distribution in FRF analysis.

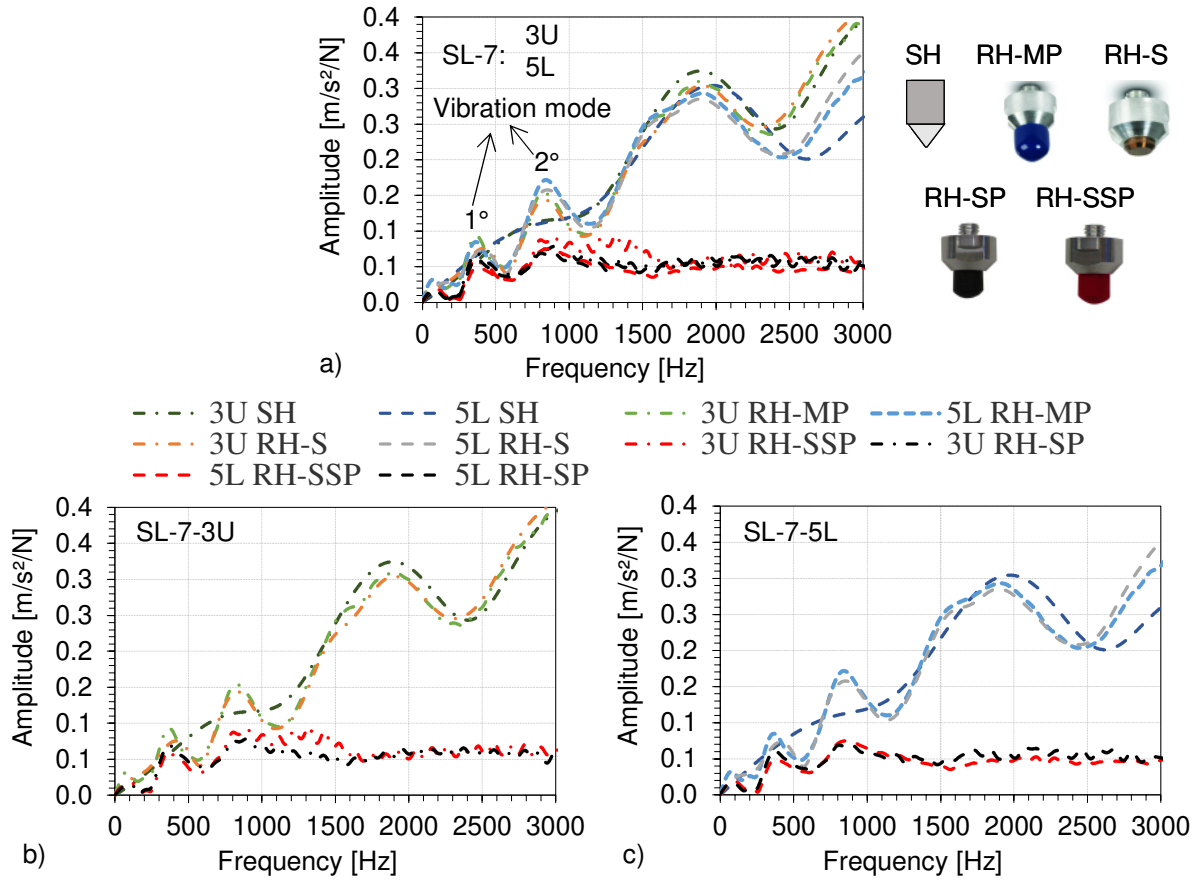

Fig. 11 Experimental FRF for tests SL-7-5L and SL-7-3U using regular hammer (RH) with four impacting tips and small hammer (SH): a) Positions 3U and 5L; b) Position 3U; c) Position 5L

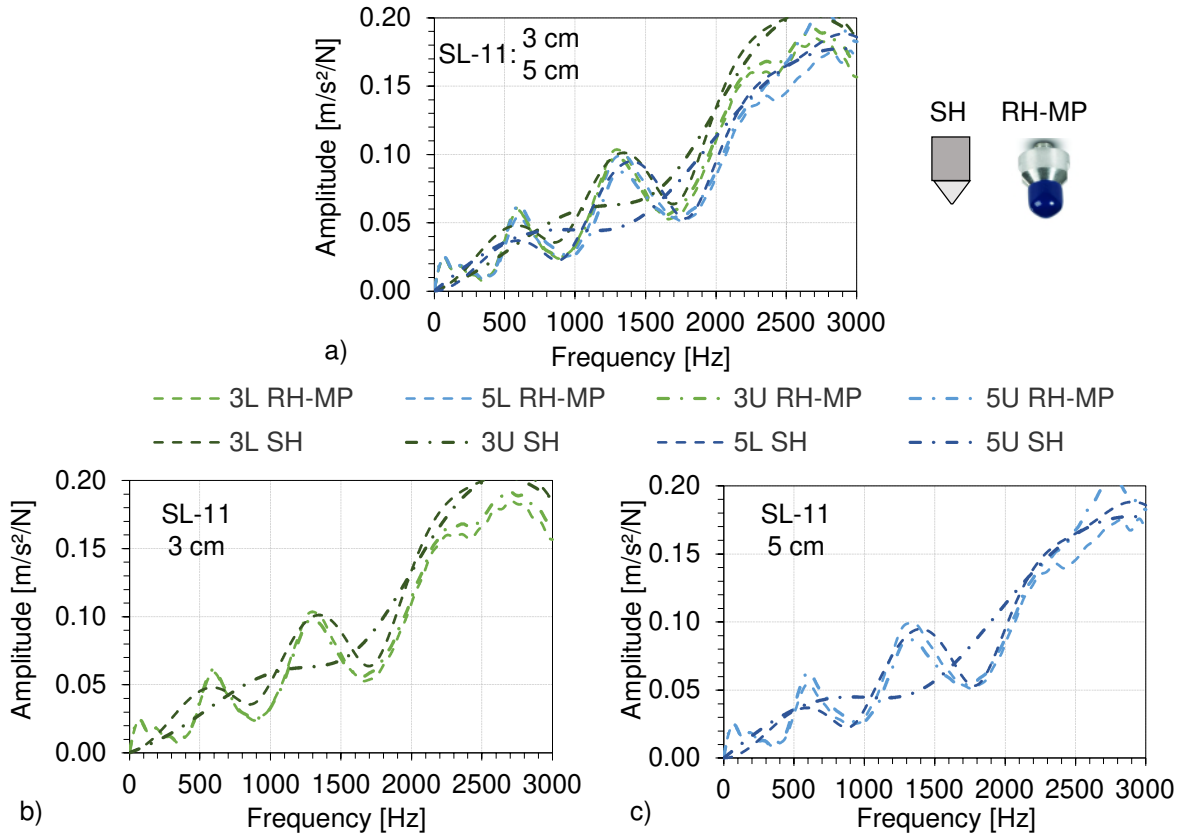

Fig. 12 Experimental FRF for tests SL-11-5L, SL-11-5U, SL-11-3U and SL-11-3L using regular hammer RH-MP and small hammer (SH): a) Positions 3U, 3L, 5U and 5L; b) Position 3U and 3L; c) Position 5L and 5U

More specifically, among the RH configurations, the RH-S and RH-MP hammers provide very similar FRF responses in the analyzed frequency range (0–3000 Hz). Both are able to excite the first two resonance peaks below 1000 Hz, which are associated with the fundamental flexural modes of the slab. This confirms that the regular hammer, combined with either the steel or medium plastic tip, provides sufficient excitation energy in the low-frequency range of interest. Overall, the results show that the RH-S and RH-MP hammers are the most suitable configurations for this slab geometry and frequency range. The SH hammer is less appropriate for identifying the first flexural modes, while RH-SP and RH-SSP provide insufficiently defined FRFs for reliable modal interpretation.

In contrast, the RH-SP and RH-SSP hammers show similar behavior to each other, but their responses are clearly different from those obtained with RH-S and RH-MP. These softer tips produce lower FRF amplitudes over the whole frequency range and do not clearly define the same resonance peaks. This behavior is consistent with their longer contact duration and lower effective excitation bandwidth, which concentrate the input energy at very low frequencies and reduce the quality of the response for identifying the slab vibration modes.

The comparison between the 3U and 5L positions also shows good repeatability regarding the obtained resonance frequencies, with very similar results independently of the analyzed position, considering the positions closer to the impact point. These results confirm that both hammer mass and tip stiffness directly control the effective excitation bandwidth and the vibration modes of the material in the rectangular slab geometry. Among the tested configurations, the RH-MP hammer appears to provide the best balance between low-frequency excitation and overall FRF quality for the slab geometry investigated in this study.

Fig. 13 presents the coherence functions obtained for all tested hammers (RH-MP, RH-S, SH, RH-SP and RH-SSP) for slab SL-7 considering the 5L position and the average of five impacts. In general, all hammers exhibit high coherence values at low frequencies, indicating good repeatability of the impacts and a strong linear relationship between the excitation and the measured response in this frequency range. However, as the frequency increases, the coherence progressively decreases, especially for the hammers equipped with softer tips (RH-SP and RH-SSP). This confirms the limited high-frequency excitation capability of these hammer configurations, as previously observed in the force and acceleration FFT results.

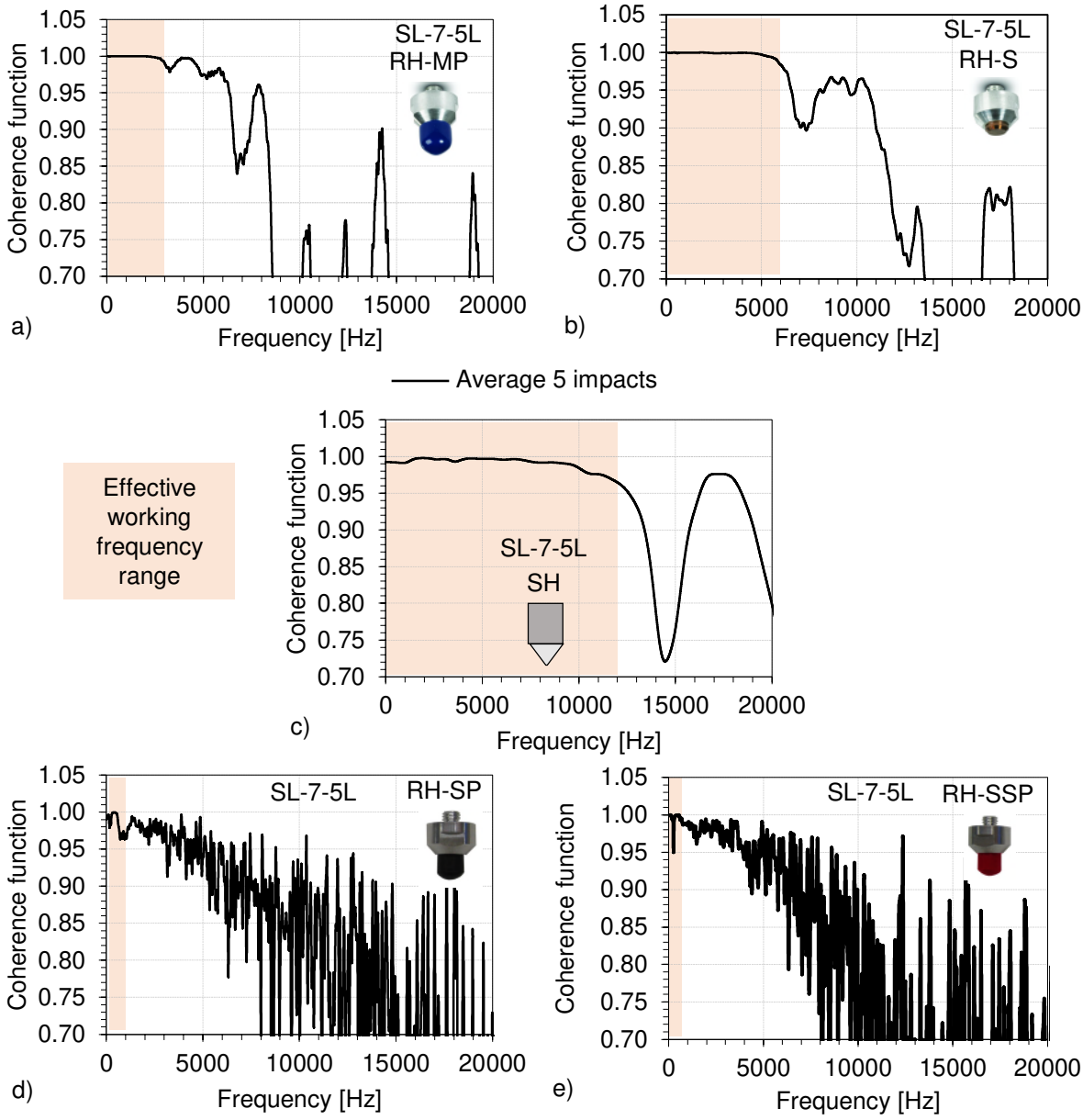

Fig. 13 Coherence function for SL-7-5L test using regular hammer (RH) with four impacting tips and small hammer (SH) at: a) RH-MP; b) RH-s; c) SH; d) RH-SP; e) RH-SSP

For the SH hammer, coherence values remain close to 1 over a much wider frequency range, confirming its ability to excite higher vibration modes due to its short contact time and high tip stiffness. The RH-S hammer also maintains relatively high coherence over an intermediate frequency range, while the RH-MP presents satisfactory coherence mainly below approximately 3 kHz. In contrast, RH-SP and RH-SSP exhibit a significant coherence reduction at lower frequencies, indicating that the excitation energy

becomes insufficient for reliable measurements at higher frequencies. These results confirm the effective excitation bandwidth previously identified for each hammer configuration and reinforce the direct relationship between hammer tip stiffness, contact time and usable frequency range in IRT experiments on bituminous mixtures.

4.1 Analysis of different measurement positions and thickness influence

Fig. 14 present the FRFs obtained with the RH-MP hammer for the two investigated slabs: SL-7 and SL-11. For each slab, the acceleration was measured at positions located at 3, 5, 10, 15, 20 and 25 cm from the impact point, in the four directions (up, down, right and left). The two slabs presented the same global behavior and good repeatability between the analyzed positions, confirming the consistency of the adopted experimental procedure.

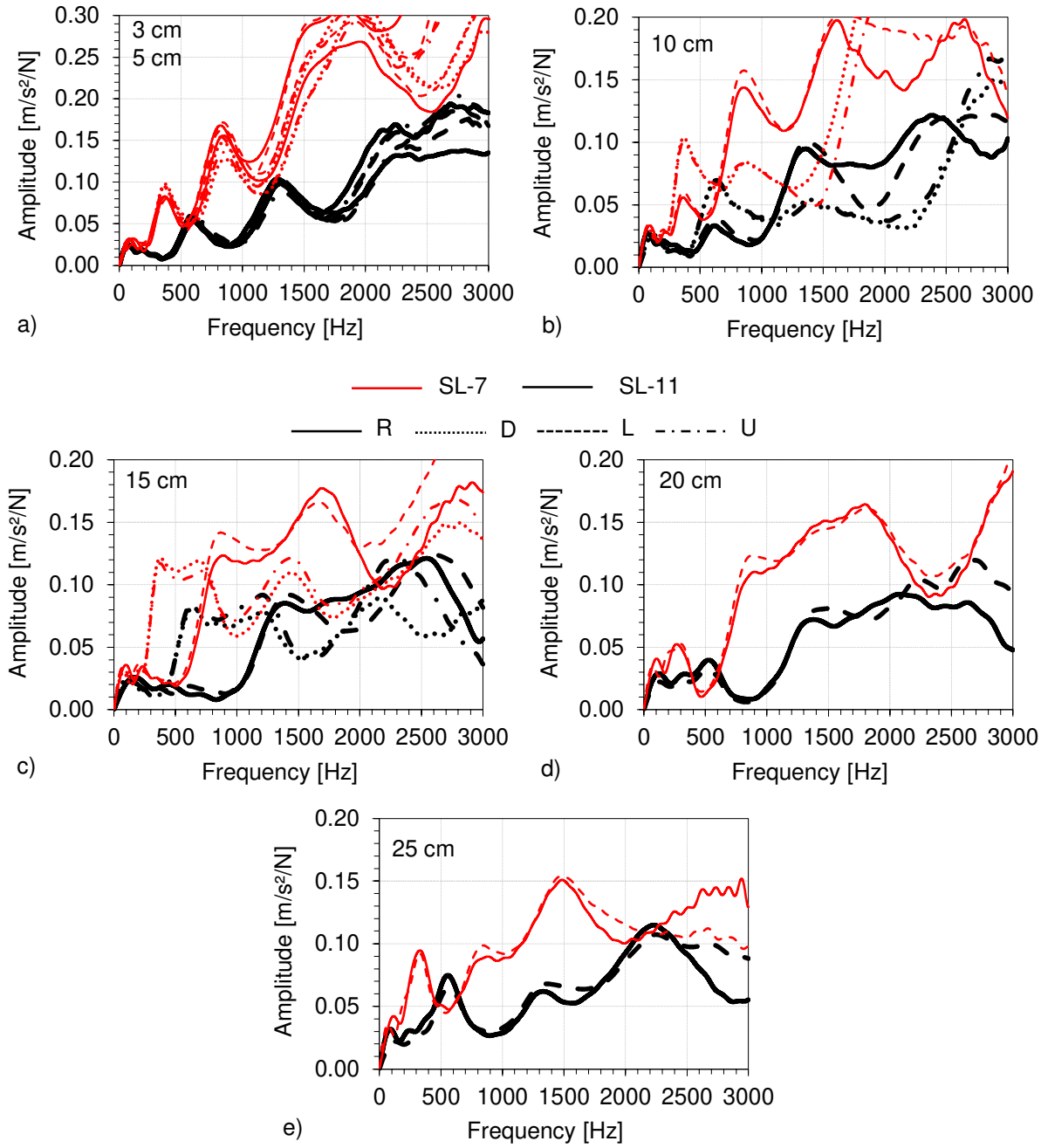

Fig. 14 Comparison of FRF for slabs, SL-7 and SL-11, with different thicknesses tested with RH-MP hammer, from the acceleration measured at different distance from the impact: a) 3 and 5 cm; b) 10 cm; c) 15 cm; d) 20 cm; e) 25 cm

The results show a significant influence of slab thickness on the vibrational response of the system, specifically on the resonance frequencies associated with the first two flexural modes. The slabs with smaller thickness present higher resonance frequencies and amplitudes, while the increase in thickness results in a shift of the peaks toward lower frequencies and in more damped responses.

It is possible to clearly observe the influence of edge effects on the vibrational response of the slabs. Up to approximately 10 cm from the impact point, the FRFs remain relatively similar, mainly regarding the first two flexural vibration modes, indicating that this region corresponds to the maximum deformation area. However, for the 20 cm and 25 cm positions, more pronounced differences begin to appear in the FRFs, especially in terms of amplitude and definition of the resonance peaks. This behavior becomes more evident due to the proximity to the slab edges, where wave reflections and interactions between the global vibration modes and local boundary effects occur. Similar results were numerically observed, confirming the influence of the edges on the vibrational response of the analyzed rectangular geometry.

At the 15 cm position, a particular behavior is observed for the first vibration mode, which appears highly damped or practically absent in some cases, while the second mode remains clearly identifiable. This result suggests that this position is close to a nodal region or minimum deformation area associated with the first flexural mode of the slab. On the other hand, the second flexural mode still presents sufficient deformation to be detected. Therefore, the results indicate that positions located up to approximately 10 cm from the central impact are more suitable for identifying the first two flexural modes of the slab.

This observation is consistent with the classical theory of thin plate vibration, in which the natural frequencies mainly depend on the flexural stiffness of the structure, the mass distribution and the boundary conditions. In general, the increase in thickness simultaneously modifies the stiffness and mass of the slab, directly changing its dynamic response and resonance frequencies. The presented results, in addition to suggesting edge reflection effects previously discussed, also indicate the presence of phenomena related to surface wave propagation. At positions further from the impact point, mainly at 20 and 25 cm, the FRFs become more complex, indicating a contribution of wave propagation along the slab surface. This behavior is consistent with the propagation of Rayleigh waves, frequently observed in asphalt materials and pavement structures subjected to dynamic impacts [4,25-26].

5 Numerical Results and Discursions

Fig. 15 presents the results of the numerical FRF obtained for all positions and directions investigated for the two slabs, SL-7 and SL-11. The numerical results are in good agreement with the experimental analyzes previously presented (Section 4.1), which also showed that the central region (up 10 cm from the impact) of the slab is the most suitable for exciting and identifying the first global flexural vibration modes, while the positions close to the edges are more influenced by boundary effects and by the propagation/reflection of surface waves.

Considering the comparison results between experimentally FRF (SH and RH-MP hammer) and the numerical FRF presented in Fig. 16 for both slabs, SL-7 e SL-11, it is confirmed that the frequency range between 0 and 3000 Hz concentrates the first two flexural vibration modes of the bituminous mixture for the rectangular slab geometry investigated in this study. A good agreement is also observed between the natural frequencies numerically predicted and the main peaks identified in the experimental FRFs obtained with the RH-MP hammer, reinforcing that this frequency range and hammer configuration is the most appropriate for the vibration mode analysis of this type of specimen. Another interesting result observed in Fig. 16c, which also shows the same trend experimentally and numerically, is the confirmation that thickness is an important geometric parameter in defining the dynamic response

of the slab. It is possible to observe that thickness influences both the position of the resonance peaks and the amplitude of the FRF.

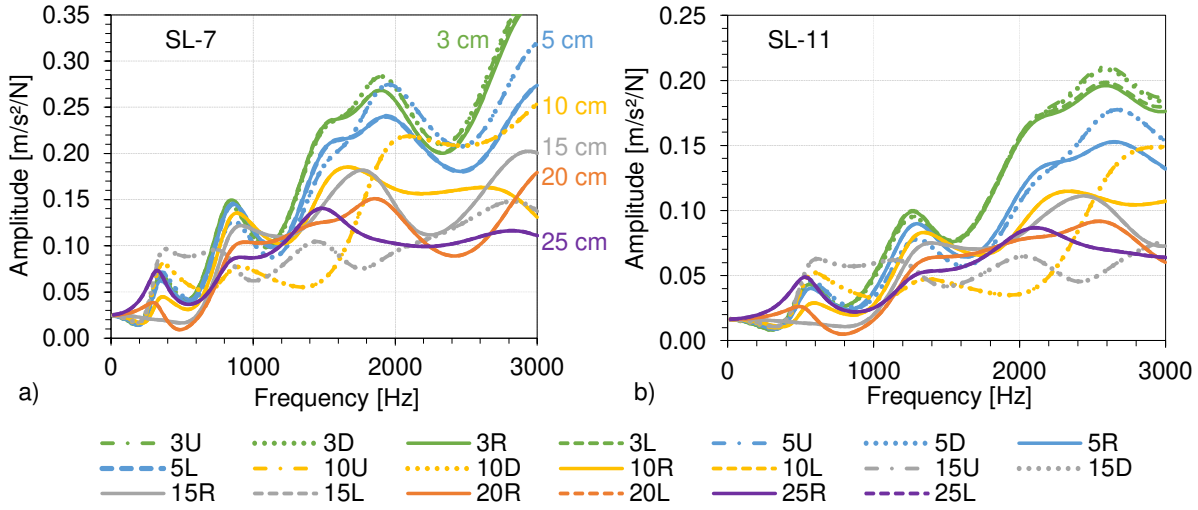

Fig. 15 Numerical FRF at 3, 5, 10, 15, 20, and 25 cm to the left (L), right (R), up (U) and down (D) of the impact.: a) for slab SL-7; b) for slab SL-11

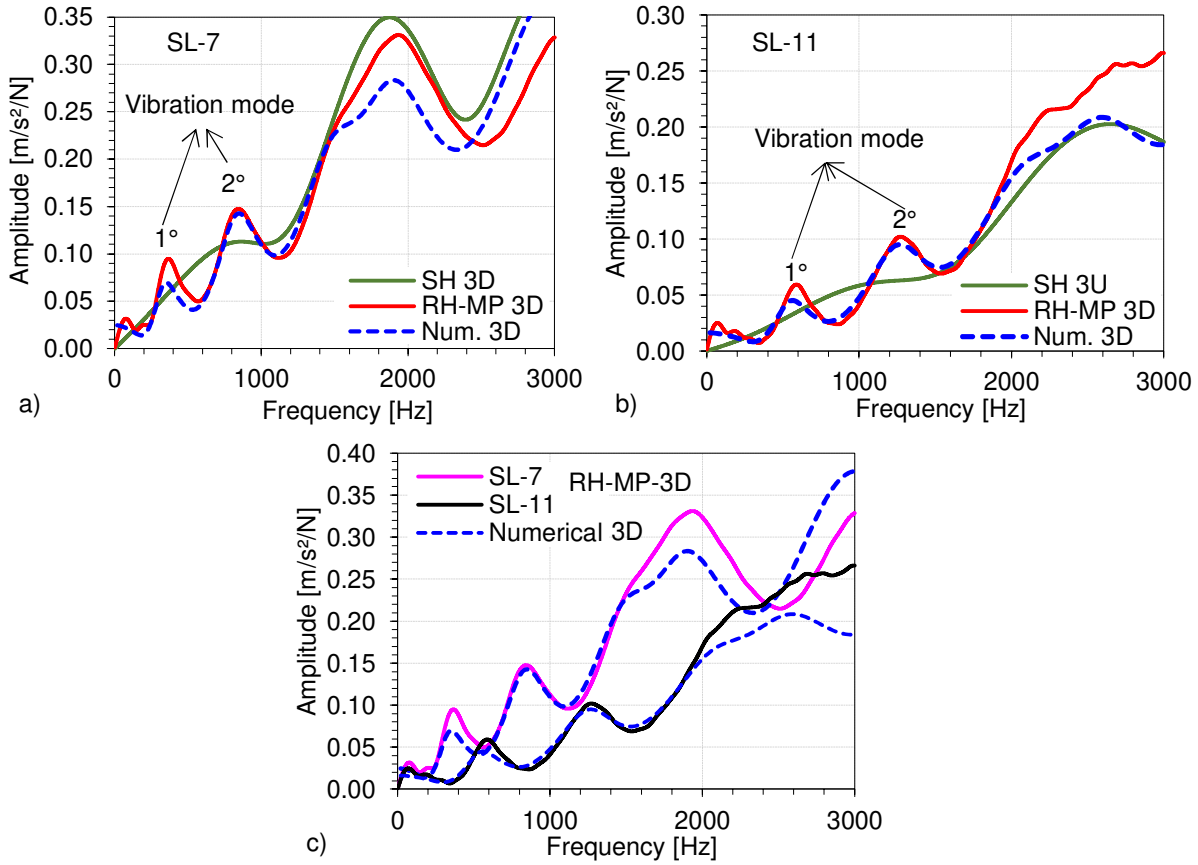

Fig. 16 Comparison between numerical and experimental FRF (for SH and RH-MP hammers) for one position: a) for slab SL-7 at position 3D; b) for slab SL-11 at position 3D (RH-MP) and 3U (SH); c) Comparison of FRF for slabs, SL-7 and SL-11, with different thicknesses tested with RH-MP hammer at position 3D

6 Conclusions

This study investigated the influence of different impact hammer configurations on the frequency response of rectangular bituminous mixture slabs using the non-destructive IRT test. Experimental measurements performed on two slabs with different thicknesses were complemented by finite element simulations to support the interpretation of the measured responses and to validate the vibration modes excited under different impact hammer configurations. Based on the obtained results, the following conclusions were obtained:

- The experimental results demonstrated that hammer mass and tip stiffness directly control the effective excitation bandwidth and, consequently, the identification of the slab vibration modes. Among the investigated configurations, the RH-MP and RH-S hammers provided the most suitable frequency content for the investigated range (0–3000 Hz), allowing clear identification of the first two flexural vibration modes. In contrast, the SH hammer showed limitations in exciting low frequencies, whereas the RH-SP and RH-SSP hammers concentrated most of their energy at very low frequencies because of their longer contact time.
- Among all tested configurations, the RH-MP hammer proved to be the most suitable for the investigated slabs, as it excites the frequency range in which the dominant flexural modes are concentrated with greater energy. These results highlight the importance of selecting an appropriate hammer configuration, considering hammer mass, tip material and impact characteristics, to ensure that the vibration modes of interest are effectively excited and correctly identified during IRT measurements of bituminous mixture slabs.
- Good agreement was observed between the experimental and numerical results, demonstrating that the numerical model based on the linear viscoelastic model adequately reproduced the dynamic response of the slabs and correctly identified the vibration modes observed experimentally. The numerical analyses also contributed to the interpretation of the measured FRFs by clarifying the influence of the excitation system on the modal response.
- The numerical and experimental results showed good repeatability among the different accelerometer positions close to the impact point, especially up to approximately 10 cm from the center of the slab. At positions further from the impact point (20 cm and 25 cm), a greater influence of edge effects and surface wave propagation/reflection was observed. The position at 15 cm presented a typical nodal-region behavior for the first flexural mode. The experimental results were consistent with the numerical simulations and indicated that positions close to the impact point are more suitable for identifying the main flexural modes in rectangular slab geometries.
- The results confirmed that the dynamic response of rectangular bituminous mixture slabs is dominated by flexural vibration modes concentrated within the frequency range between 0 and 3000 Hz. In addition, slab thickness influenced the resonance frequencies, with the thicker slab exhibiting lower resonance frequencies while preserving the same overall trends observed for the different hammer configurations. The repeatability of these trends on both slabs supports the consistency of the proposed experimental approach.

References

[1] Whitmoyer SL, Kim YR (1994) Determining asphalt concrete properties via the impact resonant method. J Test Eval 22(2):139–148. https://doi.org/10.1520/JTE12648J

[2] Di Benedetto H, Sauzéat C, Sohm J (2009) Stiffness of bituminous mixtures using ultrasonic wave propagation. Road Mater Pavement Des 10(4):789–814. https://doi.org/10.1080/14680629.2009.9690227

[3] Mounier D, Di Benedetto H, Sauzéat C (2012) Determination of bituminous mixtures linear properties using ultrasonic wave propagation. Constr Build Mater 36:638–647. https://doi.org/10.1016/j.conbuildmat.2012.04.136

[4] Gudmarsson A, Rydén N, Birgisson B (2012) Application of resonant acoustic spectroscopy to asphalt concrete beams for determination of the dynamic modulus. Mater Struct 45(12):1903–1913. https://doi.org/10.1617/s11527-012-9877-3

[5] Carret J-C, Pedraza A, Di Benedetto H, Sauzéat C (2018) Comparison of the 3-dim linear viscoelastic behavior of asphalt mixes determined with tension-compression and dynamic tests. Constr Build Mater 174:529–536. https://doi.org/10.1016/j.conbuildmat.2018.04.156

[6] Carret J-C, Babadopulos L (2025) Opening letter of RILEM TC MWP: Mechanical wave propagation to characterize bituminous mixtures. RILEM Tech Lett 10:15–21. https://doi.org/10.21809/rilemtechlett.2025.211

[7] Gudmarsson A, Rydén N, Di Benedetto H, Sauzéat C (2015) Complex modulus and complex Poisson's ratio from cyclic and dynamic modal testing of asphalt concrete. Constr Build Mater 88:20–31. https://doi.org/10.1016/j.conbuildmat.2015.04.007

[8] Carret J-C, Di Benedetto H, Sauzéat C (2018) Characterization of asphalt mixes behaviour from dynamic tests and comparison with conventional cyclic tension–compression tests. Appl Sci 8(11):2117. https://doi.org/10.3390/app8112117

[9] Carret J-C, Di Benedetto H, Sauzéat C (2020) Linear viscoelastic behavior of asphalt mixes from dynamic frequency response functions. Int J Numer Anal Methods Geomech 44(7):1019–1031. https://doi.org/10.1002/nag.3045

[10] Kim YR, Lee Y-C (1995) Interrelationships among stiffnesses of asphalt-aggregate mixtures. J Assoc Asphalt Paving Technol 64:575–609.

[11] Kweon G, Kim YR (2006) Determination of asphalt concrete complex modulus with impact resonance test. Transp Res Rec 1970(1):151–160. https://doi.org/10.1177/0361198106197000119

[12] Kim D, Kim YR (2017) Determination of dynamic modulus values of asphalt mixtures using impact resonance testing of thin disk specimens. J Test Eval 45(2):509–520. https://doi.org/10.1520/JTE20150076

[13] Rydén N (2011) Resonant frequency testing of cylindrical asphalt samples. Eur J Environ Civ Eng 15(4):587–600. https://doi.org/10.1080/19648189.2011.9693349

[14] Mun S (2015) Determining the dynamic modulus of a viscoelastic asphalt mixture using an impact resonance test with damping effect. Res Nondestruct Eval 26(4):189–207. https://doi.org/10.1080/09349847.2015.1023914

[15] Zahari SN, Sani MSM (2011) Investigation on impact hammer testing with different types of hammer tip for welded thin plate. Adv Sci Lett 4(2):400–407. https://doi.org/10.1166/asl.2011.1261

[16] Mali KD, Singru PM (2018) Study on the effect of the impact location and the type of hammer tip on the frequency response function (FRF) in experimental modal analysis of rectangular plates. IOP Conf Ser Mater Sci Eng 330:012102. https://doi.org/10.1088/1757-899X/330/1/012102

[17] Dvořák R, Topolář L (2021) Effect of hammer type on generated mechanical signals in impact-echo testing. Materials 14(3):606. https://doi.org/10.3390/ma14030606

[18] Corté J-F, Di Benedetto H (2005) Matériaux routiers bitumineux 1: Description et propriétés des constituants. Hermes-Lavoisier, Paris

[19] Di Benedetto H, Partl MN, Francken L, De La Roche Saint André C (2001) Stiffness testing for bituminous mixtures. Mater Struct 34:66–70. https://doi.org/10.1007/BF02481553

[20] Ministère des Transports du Québec (2024) LC 26-400: Fabrication d'éprouvettes au compacteur LCPC. Ministère des Transports du Québec, Québec

[21] Olard F, Di Benedetto H (2003) General "2S2P1D" model and relation between the linear viscoelastic behaviours of bituminous binders and mixes. Road Mater Pavement Des 4(2):185–224. https://doi.org/10.1080/14680629.2003.9689946

[22] Di Benedetto H, Delaporte B, Sauzéat C (2007) Three-dimensional linear behavior of bituminous materials: Experiments and modeling. Int J Geomech 7(2):149–157. https://doi.org/10.1061/(ASCE)1532-3641(2007)7:2(149)

[23] Williams ML, Landel RF, Ferry JD (1955) The temperature dependence of relaxation mechanisms in amorphous polymers and other glass-forming liquids. J Am Chem Soc 77(14):3701–3707. https://doi.org/10.1021/ja01619a008

[24] Bolognese M, Greco E, Bianco F, Licitra G (2025) Dynamic stiffness measurements of road pavements by means of impact hammer in a non-resonant configuration. Appl Sci 15(2):651. https://doi.org/10.3390/app15020651

[25] Rydén N (2004) Surface wave testing of pavements. Doctoral thesis, Department of Engineering Geology, Lund Institute of Technology, Lund University, Lund

[26] Meng A, Xu H, Feng X, Tan Y (2020) Feasibility of freeze-thaw damage analysis for asphalt mixtures through dynamic nondestructive testing. Constr Build Mater 233:117220. https://doi.org/10.1016/j.conbuildmat.2019.117220

Statements and Declarations

Funding

This work was supported by European Union's Horizon Europe programme under the Marie Skłodowska-Curie under Grant No. 101072820.

Competing Interests

The authors have no relevant financial or non-financial interests to disclose.

Author Contributions

Conceptualization: AKLB, JCC, SM, CS; Methodology: AKLB, JCC, SM, CS; Investigation: AKLB, JCC, SM, CS; Formal analysis: AKLB; Writing—original draft: AKLB; Writing—review and editing: AKLB, JCC, SM, CS; Supervision: CS, SM, JCC. All authors read and approved the final manuscript.

Data Availability

Data are available from the corresponding author on reasonable request.